JOURNAL OF CATALYSIS 108, 112–134 (1987)

Mössbauer Spectroscopic Investigations of Bimetallic FeCo, FeNi, and FeRu Model Catalysts Supported on Magnesium Hydroxide Carbonate

K. NAGORNY[1] AND S. BUBERT

Institute of Physical Chemistry, University of Hamburg, Bundesstrasse 45, D-2000 Hamburg 13, Federal Republic of Germany

Received May 8, 1984; revised March 25, 1987

FeCo, FeNi, and FeRu alloys supported on basic magnesium carbonate have been prepared by precipitation from salt solutions at 340 K onto the support using ion exchange and have been subsequently annealed for 20 h under argon. The particle size of the metal/support compounds could be controlled by choosing different decomposition temperatures. The surface area determined by the BET method depended both on the decomposition temperature and on the alloying component, which points toward different metal–support interactions.

The reduction, oxidation, and sintering behavior of the samples under H_2 or CO exposure has been investigated at 723 K by means of Mössbauer spectroscopy. Quantitative evaluation of the spectra has permitted determination of the kinetics of the reactions with H_2 and with CO. For quantitative Mössbauer spectroscopic analysis it proved to be necessary to determine the Debye temperatures, which were different and considerably lowered compared to less dispersed solids. The comparison of the resonance absorption areas of the spectra taken at 4 and 295 K allowed the calculation of the Debye temperatures and Debye–Waller factors of the different components. From the Debye–Waller factors the relative fractions could be extrapolated to the conditions at 0 K. The kinetics of the H_2 exposure showed an increase in the reduction velocity as well as in the degree of reduction in the sequence FeCo < FeNi < FeRu. Above a critical particle diameter a phase separation occurred because of the segregation of an iron-rich phase at the surface of the alloy particles. The kinetics of the CO exposure demonstrated that with FeCo clusters iron(III) surface oxide layers form, whereas with FeNi clusters iron(II) surface oxide layers are generated. FeCo clusters with a cobalt content of 25% form only unstable surface carbides, whereas clusters with a cobalt content of about 5% form stable bulk carbides. The velocity of carbide formation increases with decreasing particle size. Based on the present data a model is proposed which explains the behavior of FeMe/magnesium hydroxide carbonate catalysts in H_2 and CO atmospheres.

INTRODUCTION

The preparation of model catalysts of well-defined structure and the investigation of their chemical and physical properties are of fundamental importance for the understanding of the Fischer–Tropsch (F.T.) synthesis and the product selectivity of the catalysts. The preparation of model catalysts and the investigation of their behavior in H_2 and CO atmospheres are reported in this paper; the results have led to the development of a model which explains a variety of processes such as reduction, oxidation, carbide formation, charge transfer, phase separation, sintering stability, and redispersion.

The number of publications which have appeared recently dealing with the preparation, H_2 and CO treatment, and product analysis of supported metal catalysts is extraordinarily large.

Important work in the field of F.T. catalysts was done by Garten and Ouis (*1, 2*), who investigated bimetallic clusters in reduced $PdFe/Al_2O_3$ catalysts by means of Mössbauer spectroscopy, and by Boudart *et al.* (*3*), who studied the properties of ex-

[1] To whom correspondence should be addressed.

0021-9517/87 $3.00

tremely small iron particles on magnesium hydroxide carbonate. A high selectivity toward the formation of propylene on supported FeRu catalysts was reported by Vannice *et al.* (*4*), whereas Ott *et al.* (*5, 6*) focused on the role of surface carbon, forming during the synthesis on unsupported FeRu. Chemisorption of CO on Ru was evidenced by Reed *et al.* (*7*) using LEED and Auger spectroscopy. Wise and McCarty (*8*) showed for the same adsorption system that the Ru–C bond is energetically more favorable than the C–C bond and that for this reason the C atoms bound by ruthenium remain isolated and do not form graphite layers.

Further investigations of FeRu on SiO_2 (*9–13*) and on Al_2O_3 (*9*) have been carried out by various authors because of the extremely strong catalytic activity of both metals.

Iron alloys with nickel and cobalt, mainly supported on SiO_2, have been studied by Raupp and Delgass (FeNi) (*14–16*), Unmuth *et al.* (FeNi, FeCo) (*17, 18*), Stanfield and Delgass, and Arcuri *et al.* (FeCo) (*19, 20*). The reducibility of NiFe on TiO_2 and Al_2O_3 was studied by Jiang *et al.* (*21*), who reported the surprising behavior that NiFe particles sinter on TiO_2 in spite of strong metal–support interaction (SMSI). Yoshioka *et al.* (*22*) observed that the metal–support interactions (MSI) increase with the increasing porosity of the support material, whereas the reducibility of the metal decreases.

The kinetics of the uptake and reaction of CO in relation to carbon deposit on the surface iron carbides in the bulk material was investigated first by Bianchi *et al.* (*23, 24*) on Fe/Al_2O_3 catalysts using Mössbauer spectroscopy. These kinetic studies were extended to Fe/SiO_2 by Tau *et al.* (*25*), giving special attention to the conversion of the different carbides into each other, and also to Fe/TiO_2 (*26*), of interest because of SMSI, where the effects of various reduction temperatures (558, 723, 773 K) were demonstrated.

Deactivation may occur in three ways:

—carbon deposit

$$2CO \rightarrow C + CO_2 \qquad [1]$$

$$H_2 + CO \rightarrow C + H_2O \qquad [2]$$

—carbide formation
—metal sintering.

Carbon deposits block the active surface of the metal catalyst, whereas carbide formation does not act implicitly in a deactivating way, but changes significantly the product selectivity. Sintering decreases the metal surface area and leads rapidly to a deactivation of the catalyst above 723 K. Sintering may be enhanced by a zeolite matrix (*3*).

It is not yet clear whether carbide formation leads to deactivation. The linear correlation between carbide formation and F.T. activity found by Raupp and Delgass (*16*) could not be confirmed either by Amelse *et al.* (*27*) or by Niemantsverdriet *et al.* (*28, 29*). They observed that the maximum activity occurred significantly before the conversion of all α-iron to carbide. As pointed out already by Vannice (*30*) the CO/H_2 reaction is of first order with regard to H_2, but is of almost zero order with respect to CO. Because of these results and the *in situ* Mössbauer studies of Niemantsverdriet *et al.* (*31, 32*), which showed that with increasing CO/H_2 ratio carbides and surprisingly large quantities of surface oxides are forming, the highest catalytic activity is obtained with a $CO : H_2$ ratio between 1 : 3 and 1 : 10.

The aim of the present work has been the preparation and investigation of iron alloy model catalysts supported on magnesium hydroxide carbonate and the study of the $CO–H_2$ reaction. We wished to determine the kinetics from the quantitative analysis of the Mössbauer spectra. For this analysis we assumed that the surface components show Debye–Waller factors deviating from that of the bulk material (*33–35*). These were measured by comparison of characteristic Mössbauer spectra at 4 and 295 K,

allowing the evaluation of the Debye temperatures.

The Debye temperature is given by

$$\theta_D = \left[\frac{-3E_\gamma^2}{Mck_B[d \ln A(T)/dt]}\right]^{0.5}.$$

A is the area under the resonance line. For calculating the Debye–Waller factors we used the following approximation:

$$\text{for } \left(T > \frac{\theta_D}{2}\right) \quad f = \exp\left[-\frac{3E_\gamma^2 T}{K_B M c^2 \theta_D^2}\right]$$

and

$$\text{for } (T \to 0)$$

$$f = \exp\left[-\frac{E_\gamma^2}{2Mc^2 K_B \theta_D}\left\{1.5 + \left(\frac{\pi T}{\theta_D}\right)^2\right\}\right].$$

The use of the Debye model has some limitations and problems which have already been itemized by Niemantsverdriet *et al.* (*35*).

EXPERIMENTAL

a. Preparation of Catalyst

The iron–alloy catalysts were prepared in the manner described by Boudart *et al.* (*3*) by the overall ion exchange reaction of magnesium hydroxide carbonate (MHC) powder [$4MgCO_3 \cdot Mg(OH)_2 \cdot 5H_2O$] obtained from Riedel-De Haën AG, Seelze, Hannover, and metal nitrate and chloride salts, respectively, from Merck. The filtered product was dried in air for 2 h at room temperature, 7 h at 320 K, and 12 h at 360 K. The notation adopted for the catalysts, for instance 5Fe5Ni/MgO, refers to 5 wt% Fe and 5 wt% Ni, respectively, measured for a decomposed and reduced sample.

Using highly enriched iron-57, we obtained a ^{57}Fe content of ca. 30 wt% ^{57}Fe referred to the whole iron content.

The dried samples were heated in quartz tubes at 673, 873, and 1073 K for 20 h under argon ($\leqq$5 vpm O_2, $\leqq$4 vpm H_2O, and purified by silica gel/Al_2O_3 and a molecular sieve 0.5 nm). Temperatures could be controlled with an accuracy of ±5K. Samples were then exposed to hydrogen, and after 8 h in H_2 flow were exposed to CO. The H_2 and the CO exposures were carried out at 723 K. We investigated the samples which had been exposed for different periods of time to H_2 and CO by Mössbauer spectroscopy at room temperature. The reaction kinetics were inferred from a quantitative analysis of the spectra. All catalysts were cooled under protecting gas and measured at room temperature. No alteration of the catalysts was observed.

b. Mössbauer Spectra

Constant acceleration spectra were obtained with an Elscint Mössbauer spectrometer and a proportional counter using a ^{57}Co source diffused into a copper matrix. The natural linewidth was theoretically 0.2 mm/s. Isomer shifts are reported with respect to an α-iron foil as standard absorber with the isomer shift of $\delta = -0.226$ mm/s comparing to copper.

The γ-ray data were analyzed by a Siemens 7882 computer using a least-squares fit program which fits the Lorentzian lineshapes with an iterative gradient algorithm. A Lorentz approximation could be used, because the effective thickness of the samples was smaller than one. Otherwise we had to evaluate the spectra by the approximative solution of the transmission integral. At the beginning of the fitting procedure physically justified parameters were given to the computer in order to minimize the relative deviation by the described program. In this manner we could analyze a spectrum with up to seven different components.

For low-temperature measurements we used a Leybold–Heraeus evaporating cryostat (Type VMK 3-7000). The temperature could be determined with a carbon resistor. Calibration was achieved by the use of a helium gas thermometer in the range from 2.9 to 4.5 K. An electronically controlled P-I thermostat (Leybold–Heraeus, Type ER3) enabled the temperature to be kept

constant by controlling the helium flow with an automatically working magnetic valve. An integrated heating system and a valve at the helium siphon which served for rough regulation of the helium flow further improved the accuracy of the nominal temperature. At 4 K it amounted to ±0.1 K.

RESULTS AND DISCUSSION

1. Heat Treatment under Argon

After 20 h of annealing under argon, mixed oxides form which have an inverse or disturbed inverse spinel structure (see, for example, Fig. 2a presented later). Each ferrimagnetic component of the mixed oxides of the 5Fe5Co/MHC (magnesium hydroxide carbonate) samples, annealed at 673 or 873 K, shows two hyperfine fields (H = 46.71 and 47.61 T and H = 47.61 and 49.13 T, respectively). The first hyperfine field with the smaller isomer shift corresponds to the tetrahedral Fe^{3+}, the second with the larger shift corresponds to the octahedral Fe^{3+}. The samples annealed at 1073 K show a third sextet (δ = 0.73 mm/s, ΔEq = 0.33 mm/s, and 45.41 T) corresponding to Fe^{2+}. These data are in accordance with the literature regarding the MES parameters of spinels: δ(tetrahedral Fe^{3+}) < δ(octahedral Fe^{3+}) and H(Fe^{2+}) < (Fe^{3+}).

X-ray diffraction (XRD) measurements revealed the existence of $CoFe_2O_4$. Reflections from α-Fe_2O_3, however, could not be observed.

Compared to the data in the literature all the hyperfine fields show distinctly lower values. Berry and Maddock (*36*) and Petrera *et al.* (*37*) already reported such a lowering of the hyperfine fields with their Fe/MHC samples. The latter authors, who observed at room temperature hyperfine fields between 37.2 and 46.5 T, explained this by superparamagnetic relaxation according to Mørup's model. The anisotropy energy would then be $KV \leqq kT$, in which case, given small particles, lowered hyperfine fields can be observed. This explanation is supported by the existence of relatively small particles which is confirmed by the high superparamagnetic component. The particularly lowered inner magnetic fields of the mixed oxide of the 5Fe5Ru/MHC sample annealed at 1074 K (δ_1 = 0.20 mm/s, H_1 = 38.53 T, δ_2 = 0.42 mm/s, H_2 = 39.41 T, and δ_3 = 0.75 mm/s, H_3 = 38.39 T, ΔEq = 0.29 mm/s) point to relatively small particles. This was also inferred from the BET surface area measurements. While all freshly precipitated and cautiously dried samples had a specific surface area of about 36.2 m^2/g, the surface areas produced after annealing under argon showed a distinct temperature-dependent behavior. As expected, the largest surface occurs with the samples decomposed at 673 K. With increasing decomposition temperature the surfaces decrease rapidly. This confirms the results obtained by other authors.

Further, the surface area increases with a constant decomposition temperature (673 K, for example) in the sequence Co < Ni < Ru of the metal oxide exposures. The tendency of ruthenium to form smaller particles is already known. Following Petrera *et al.* (*37*), an alternative explanation for the decrease in the hyperfine fields would be local inhomogeneities in the composition of the mixed oxide. Mixed oxides form with magnesium hydroxide carbonate nonstoichiometric Feitknecht compounds (*38*).

Martens *et al.* (*39*) and Freund (*40*), who studied the decomposition of $Mg(OH)_2$ under vacuum, reported that below 743 K a hexagonal "defect MgO" is generated. They denoted this as $Mg(OH)_{2-x}Q_{x/2}O_{x/2}$, where Q denotes neutral vacancy sites resulting from dehydration. Freund's Monte Carlo calculations show that the x value must exceed about 1.8 (corresponding to a 90% dehydration) before the recrystallization from hexagonal "defect MgO" to cubic MgO takes place. If now parts of these defective MHC or MgO structures form mixed oxides with the metal oxides, increasing inhomogeneities and increasingly lowered hyperfine fields are expected for increasing addition of the support. The hy-

perfine fields which we observed can then be interpreted in the way that the hyperfine fields, lowered by 10 T for the 5Fe5Ru/MHC sample annealed 20 h at 1073 K, point toward a rather strong incorporation of the support into the mixed oxide. IR spectroscopic investigations of our samples resulted in an increasing decomposition temperature with increasing degree of dehydration of the support, but even after H_2 exposure the dehydration of the carrier is not completely finished.

Summarizing, we propose that the decrease in the hyperfine fields is caused by inhomogeneities in the composition due to the incorporation of MHC or MgO, respectively, into the mixed oxide, and on the other hand, by the relaxation effect.

The relatively large half-width of the sextets may be partially interpreted by a certain hyperfine field distribution, but also by defects of the spinel structure.

The superparamagnetic component represented by a doublet in the Mössbauer spectrum with isomer shifts between 0.22 and 0.34 mm/s and quadrupole splittings from 0.75 to 0.96 mm/s, showed relatively large linewidths from 0.70 to 1.02 mm/s. We assume that each doublet consists of slightly varying doublets with different quadrupole splittings. This may be understood from the fact that Mössbauer nuclei located at the corners, edges, and surfaces and in the volume have different EFG (electronic field gradients). Then, with large particles the bulk component dominates, so that the fitting by a single doublet leads to sufficiently small linewidths, whereas with small particles (surface material dominant) the fitting must be achieved by several doublets. We fitted by one doublet and had, therefore, to accept the larger linewidths. Also $Fe(NO_3)_3 \cdot 9H_2O$ samples which were only air-dried, showed these relatively large linewidths. From the investigations of Mørup and Thrane (*41*) it is known that an increase in the spin–spin relaxation time caused by the influence of neighboring atoms with different ionic states in the case of $Fe(NO_3)_3 \cdot 9H_2O$ can achieve a line broadening in the Mössbauer spectrum.

Furthermore, it was important for us to obtain criteria regarding the particle size from the Mössbauer spectra. Krupianskii and Suzdalev (*42*) correlated the quadrupole splitting of superparamagnetic γ-Fe_2O_3 with the particle size determined by X-ray structure analysis. When the anisotropy constant K is known, the particle size can be determined by measuring the superparamagnetic component at various temperatures, as reported by Kündig *et al.* (*43*). This method allows the determination of particle size from the sextet component. However, already Hobson and Gager (*44*) explained that this procedure is problematic if the iron oxide forms mixed compounds with the support. These authors assume that very small X-ray amorphous mixed oxide particles (in their case $FeAlO_3$) occur in addition to substantially larger Fe_2O_3 particles leading to large particle distributions which question the correlation between the particle size and the ratio of superparamagnetic and ferromagnetic components. Beyond that, the dependence of the Debye–Waller factor from the particle size tends to make the procedure doubtful.

In spite of all these reservations, we determined the particle size from the quadrupole splitting as well as from the sextet component in order to obtain an approximate criterion for the particle sizes. Table 1 compiles the results and correlates them with the values obtained by the BET surface area measurement. The particle size determined from the BET surface area assumes spherical shape for the primary particles.

With increasing annealing temperature not only does the mean particle diameter increase, but also the ratio of support particle diameter d_T to metal oxide particle diameter d_{MO} increases. The latter may be explained assuming that the surface area decrease in the support, is on the one hand, effected continuously by coalescence during the annealing process, and on the other

TABLE 1

Comparison of the Mean Diameter of the Support Particles d_T (from BET Surface Area) and of the Metal Oxide Particles d_{MO} (from Mössbauer Spectra) after 20 h of Decomposition under Argon at Different Temperatures

Sample:	5Fe5Co/MHC			5Fe5Ni/MHC			5Fe5Ru/MHC		
T (K):	673	873	1073	673	873	1073	673	873	1073
S.A. (m^2/g)	57.5	40.0	7.7	76.9	18.0	10.3	83.7	61.4	17.6
d_T (nm)	32.2	42.6	210.6	24.0	94.2	157.0	22.0	27.4	91.6
d_{MO} (nm)	11.5	12.0	12.5	6.5	18.0	25.0	3.2	3.5	10.0

hand—discontinuously—by the recrystallization from the hexagonal "defect MgO" to the cubic MgO. The first effect dominates at 673 and 873 K, the second at 1073 K (cf. Table 1).

Furthermore, it can be seen that the 5Fe5Ru/MHC samples at 673 and 873 K show a comparatively high stability against sintering.

2. *Low-Temperature Mössbauer Emission Spectroscopy (MES) Measurements*

Three samples were exposed to H_2 and subsequently to CO. The spectra of these samples which were taken at room temperature showed (within the limits of experimental error) no change after introduction into a "UHU-plus" matrix.

The powder samples thus fixed in a UHU-plus matrix were subsequently measured at 4 K.

The Mössbauer spectra are reproduced in Figs. 1a–1c. The upper spectrum each time has been taken at room temperature, and the lower one at low temperature. Included at the right-hand side are the corresponding spectra from computer analysis. Tables 2a–2c show the MES parameters found with the relative fractions of the individual components extrapolated to 0 K, as well as the Debye temperatures calculated according to Eq. [2]. The qualitative assignment of the systems is based on published data. All samples show a relative FeO · MgO cluster fraction of 0.08 to 0.17. The formation of clusters between Fe^{2+} and the support was known for some time.

Boudart *et al.* (*3*) denoted this formation of clusters as a solid solution of FeO in MgO. This solid solution is not homogeneous, as Boudart *et al.* could show by XRD, but there are MgO regions with high Fe^{2+} concentrations which build up in the neighborhood of the completely reduced iron.

As the increase in the Debye–Waller factor with decreasing temperature leads to an increase in the area under the resonance lines, we had to fit the resonance area of the FeO–MgO partially by a singlet, and partially by a doublet. Simkin *et al.* (*45*) showed already that Fe^{2+} with concentrations below 6% exhibits no quadrupole splitting in MgO at 298 K. The author explained this as being due to the very low Fe^{2+} concentrations, where the MgO lattice deformations are too low and the quasi-isolated Fe^{2+} ions hardly cause defects in the cubic crystal lattice.

Only with higher Fe^{2+} concentrations (>6%) does systematic cluster formation occur and an EFG is generated by the influence of the disturbed symmetrical charge distribution by neighboring Fe^{2+} ions.

In MgO 8 wt% Fe^{2+}, Bhide and Tambe (*46*) observed a quadrupole splitting of 0.30 mm/s, and for 10 wt% Shirane *et al.* (*47*) found a splitting of 0.68 mm/s. With higher Fe^{2+} concentrations the quadrupole splitting is reported to be nearly constant. While Boudart *et al.* (*3*) found a doublet with a

quadrupole splitting around 0.80 mm/s, even with 10% Fe/MgO samples, Jung *et al.* (*48*) observed with 5% Fe/Carbolac-1 samples (BET surface 950 cm^2/g) Fe^{2+} without a quadrupole splitting, represented in the MES only by a singlet with $\delta = 1.07$ mm/s. Recently, Niemantsverdriet *et al.* (*49*) reported that this singlet splits at 77 K into a doublet. They explained this by the reciprocal compensating of different contributions of opposite sign to the EFG and to the lattice field gradients.

Travis (*50*), also, discussed this way of interpretation. The contribution of the asymmetric charge distribution of the six 3*d* electrons is temperature dependent; but that of the noncubic lattice symmetry is not, so that with opposed signs of both contributions to the EFG at a certain temperature, a compensation can take place.

With our samples, Fe^{2+} shows at room temperature only a singlet, if two conditions are fulfilled: (1) the BET surface area was above 60 m^2/g, and (2) the support did not yet exist in the form of cubic MgO because of the still incomplete dehydration which would be detected by IR spectroscopic measurements. This confirms the interpretation of Niemantsverdriet *et al.*

With rather small particles we did not see a symmetric charge distribution (because of surface effects, etc.). Even the assumption of quasi-isolated Fe^{2+} ions distributed relatively uniformly in the support and without forming larger clusters seems to be problematic to us. This would contradict the diffusion models. In addition, the recrystallization of the hexagonal "defect MgO" to the cubic MgO takes place significantly only during the annealing under argon at temperatures above 900 K or during H_2 exposure. This means that the lattice field gradient compensating the EFG is generated by the hexagonal "defect-MgO." After re-

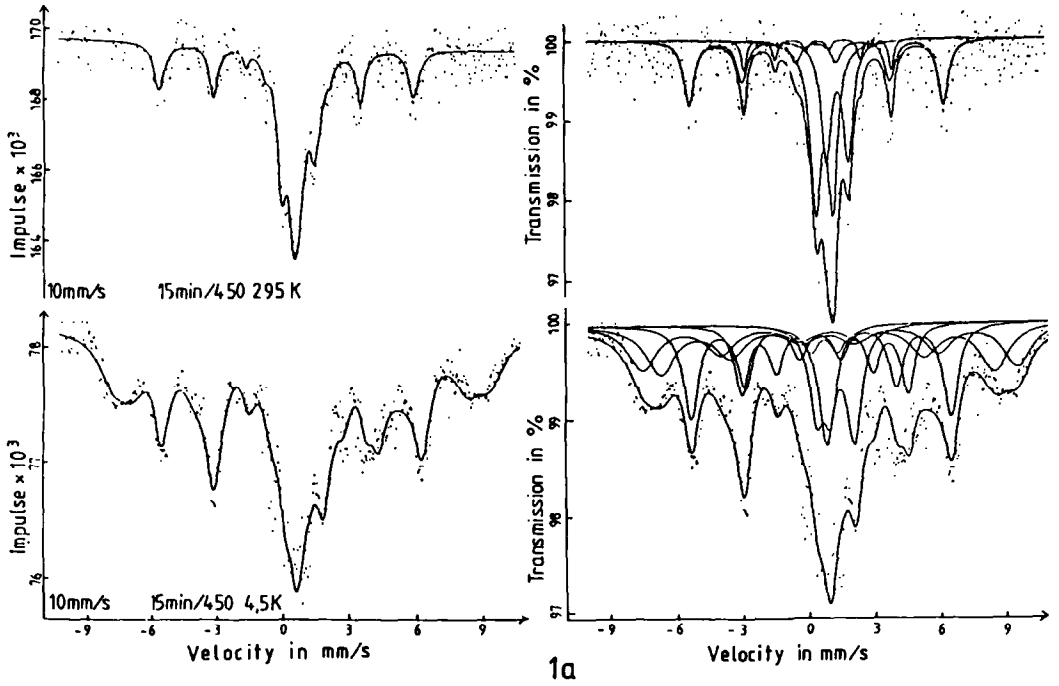

FIG. 1. Mössbauer emission spectra. (a) 5Fe5Co/MHC: 20 h/873 K/Ar, 8 h/723 K/H_2, and 15 min/723 K/CO at 295 and 4.5 K. (b) 5Fe5Ni/MHC: 20 h/673 K/Ar, 12 h/723 K/H_2, and 5 h/723 K/CO at 295 and 4.4 K. (c) 5Fe5Ru/MHC: 20 h/673 K/Ar, 8 h/723 K/H_2, and 35 min/723 K/CO at 295 and 4.4 K. Left side, measured spectra and fitting curve; right side, computer analysis of the measured spectra.

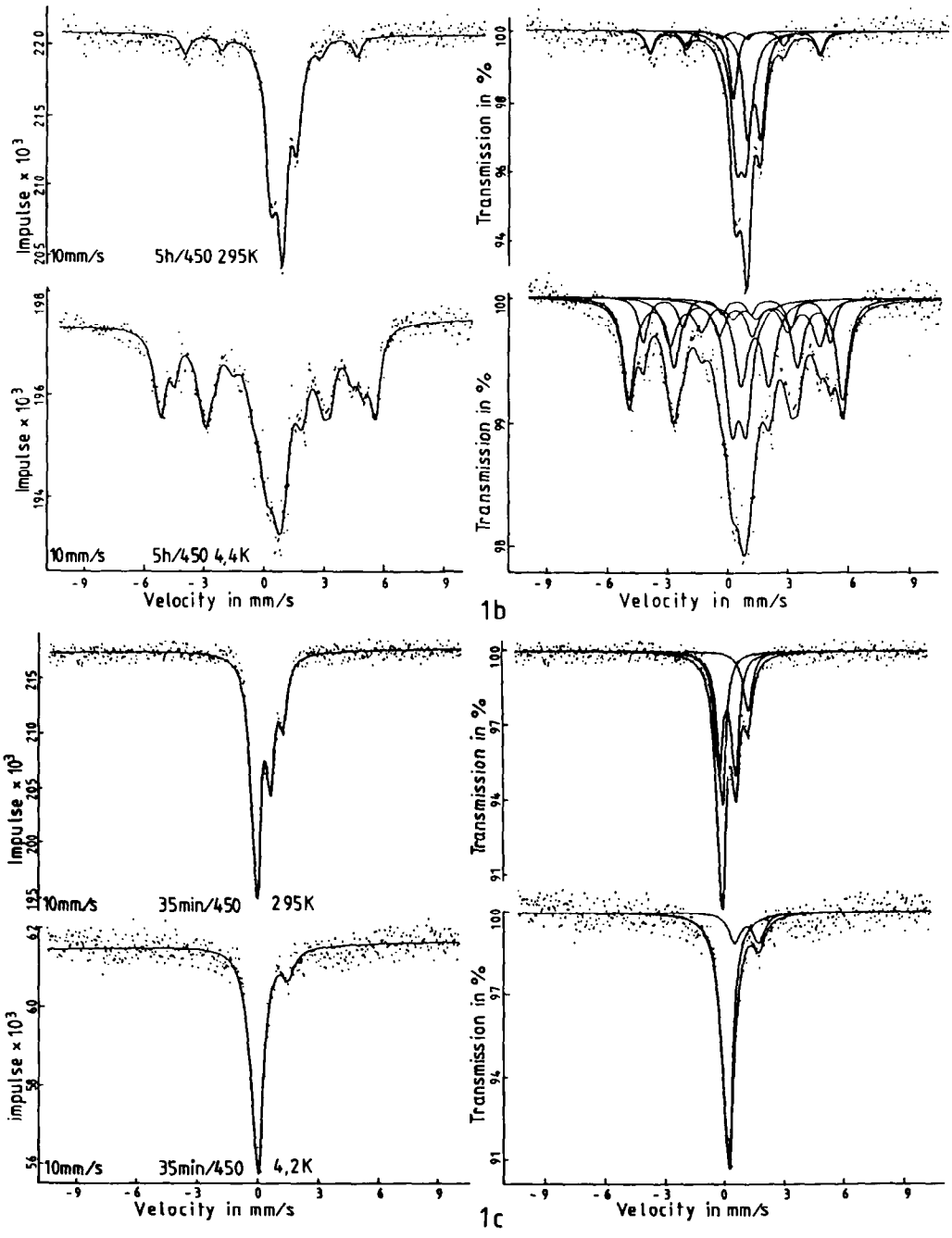

FIG. 1—*Continued.*

crystallization to the cubic MgO, the lattice field gradient is zero and, from there, the EFG is in any case different from zero. The Fe^{2+} shows a doublet. The fact that the samples of the 5Fe5Ru/MHC catalyst annealed at 1073 K also show a singlet for the Fe^{2+} can be attributed, in our opinion, to the strong interaction between the hexagonal FeRu alloy and the hexagonal "defect MgO" which decelerate a recrystallization

TABLE 2a

MES Parameters[a] of 5Fe5Co/MHC: 20 h/873 K/Ar, 8 h/723 K/H_2 and 15 min/723 K/CO

	Doublet FeO · CoO · MgO				Sextet Fe_3CO				Sextet θ-$Fe_{3-x}Co_xC$				Doublet and Sextet $Fe_xCo_yO_{1,5x+y}$				
	δ (mm/s)	Γ (mm/s)	ΔEq (mm/s)	rel[e,b]	δ (mm/s)	Γ (mm/s)	H (T)	rel[e,b]	δ (mm/s)	Γ (mm/s)	H (T)	rel[e,b]	δ (mm/s)	Γ (mm/s)	H (T)	Δ (mm/s)	rel[e,b]
295 K	0.98	0.54	0.98	0.12 (0.25)	0.10	0.56	36.06	0.22 (0.32)	0.18	0.30	20.39	0.16 (0.08)	0.37	0.57	—	0.76	0.50 (0.35)
4.5 K	0.97	0.82	1.25	0.11 (0.12)	0.15	0.79	36.51	0.21 (0.22)	0.34	0.73	23.32	0.16 (0.15)	0.20 0.48 0.59	0.76 1.57 1.54	— 46.97 52.73	0.63 —	0.09 0.22 0.21 (0.51)
Debye temp. θ_D (K)	462				273				158				179				

[a] Mean error, ±0.05 mm/s, ±0.2 T, ±5% relative to the relative contents.
[b] rel[e], relative part extrapolated to 0 K, measured values in parentheses.

TABLE 2b

MES Parameters[a] of 5Fe5Ni/MHC: 20 h/673 K/Ar, 12 h/723 K/H_2, and 5 h/723 K/CO

	Singlet/doublet FeO · MHC				Singlet/sextet Fe–(29 ± 3)% Ni				Sextet Fe–(70 ± 5)% Ni				Doublet and sextet χ-$Fe_{5-x}Ni_xC_2$				
	δ (mm/s)	Γ (mm/s)	ΔEq (mm/s)	rel[e,b]	δ (mm/s)	Γ (mm/s)	H (T)	rel[e,b]	δ (mm/s)	Γ (mm/s)	H (T)	rel[e,b]	δ (mm/s)	Γ (mm/s)	ΔEq	H (T)	rel[e,b]
295 K	1.07	0.55	0.73	0.25 (0.31)	−0.09	0.48	—	0.27 (0.11)	0.06	0.56	29.11	0.12 (0.14)	0.37	0.68	0.52	—	0.36 (0.44)
4.5 K	1.02	0.81	1.42	0.16 (0.17)	+0.08	0.70	33.33	0.31 (0.29)	0.13	0.53	29.17	0.13 (0.13)	0.19 0.53	0.78 0.80	0.73 —	— 23.40	0.20 0.20 (0.41)
Debye temp. θ_D (K)	—				182				537				560				

[a] Mean error, ±0.05 mm/s, ±0.2 T, ±5% relative to the relative contents.
[b] rel[e], relative part extrapolated to 0 K, measured values in parentheses.

TABLE 2c

MES Parameters[a] of 5Fe5Ru/MHC: 20 h/673 K/Ar, 8 h/723 K/H_2, and 35 min/723 K/CO

	Singlet/doublet FeO · MgO				Doublet Fe–xRu ($x \geqq 13\%$)				Singlet Fe–xRu ($x \geqq 13\%$)			
	δ (mm/s)	Γ (mm/s)	ΔEq (mm/s)	rel[e,b]	δ (mm/s)	Γ (mm/s)	ΔEq (mm/s)	rel[e,b]	δ (mm/s)	Γ (mm/s)	H (T)	rel[e,b]
295 K	1.34	0.55	—	0.17 (0.17)	0.27	0.48	0.84	0.50 (0.50)	0.00	0.48	—	0.33 (0.33)
4.5 K	1.11	0.73	1.21	0.17 (0.17)		—			0.05	0.66	2.0	0.83 (0.83)
Debye temp. θ_D (K)	517				502				502			

[a] Mean error, ±0.05 mm/s, ±0.2 T, ±5% relative to the relative contents.
[b] rel[e], relative part extrapolated to 0 K, measured values in parentheses.

of the latter to the cubic MgO. This, accordingly, points toward "SMSI" for the 5Fe5Ru/MHC samples. The resonance areas under the 5Fe5Co/MHC samples cannot be fitted in any case by a singlet. Based on the relatively large mean particle diameter (see Table 1) for the cobalt-containing sample and on the low stability against sintering, the following explanation is offered: the Fe^{2+} of the 5Fe5Co/MHC samples form primarily clusters with the cubic CoO, in which the support participates only to a minor extent.

This suggests that with the 5Fe5Co/MHC catalyst only weak metal–support interaction ("WMSI") occurs.

The Fe^{2+} of our samples show Debye temperatures between 462 and 550 K. These temperatures correspond to those of bulk material, which is surprising since, for example, Benziger and Larson (*51*) reported that FeO · MgO clusters are concentrated on the surface. Highly dispersed or surface atoms can, however, exhibit high Debye temperatures provided they are rather strongly bound by the support. The Debye temperature of MgO is 946 K; following the calculation of Somorjai (*33*) the Debye temperature of the surface atoms should be half the value of the bulk. Therefore, we could expect for MgO a Debye temperature of about 475 K for the FeO · MgO surface clusters. Our results are in accordance with Somorjai's theory and demonstrate the major role of coupling effects for the Debye temperatures.

The next objective to be discussed are the alloys. The spectrum of the 5Fe5Co/MHC sample measured at room temperature showed a sextet of 36.00 T. This sextet is to be attributed to the alloy that is similar to that of Fe_3Co (ca. 20 to 30% Co). All samples of the same series of measurement showed the same hyperfine field splitting within the experimental error of ±0.2 T.

The low Debye temperature of the iron–cobalt alloy points toward the existence of microparticles (≦2 nm). This is striking because we had measured for the 5Fe5Co/MHC samples particle sizes on the order of 12 nm. One possible explanation might be that during the CO exposure an intraparticle redispersion according to the model of Wang and Schmidt (*52*) has taken place. This assumption seems to be realistic because during the CO exposure large quantities of surface oxides ($Fe_xCo_yO_{1.5x+y}$) occur which following Wang and Schmidt are the reason for the intraparticle redispersion.

The 5Fe5Ni/MHC sample selected for the low-temperature measurements shows the existence of two alloy phases: that of the alloy Invar, i.e., Fe–(29 ± 3)% Ni (singlet) and that of the Fe–(70 ± 5)% Ni alloy (sextet). The singlet of the Invar alloy splits at 4 K into a sextet. This sextet corresponds to 33.33 T.

The Debye temperature of the Invar alloy of our catalyst is only half as large as that of the Fe–(70 ± 5)% Ni alloys. From this we conclude that the Invar alloy crystallizes at the surface, but the Ni-rich alloy crystallizes in the bulk. This phase separation points in our opinion toward a strong Ni–MHC interaction leading to a partial segregation of the iron at the surface.

The low-temperature Mössbauer spectrum of the 5Fe5Ru/MHC sample gives another important result. All our 5Fe5Ru/MHC catalysts measured at 295 K showed after H_2 or CO exposure a singlet with Mössbauer parameters typical for the hexagonal Fe–xRu ($x \geqq 13\%$) and a doublet with an isomer shift of $\delta \approx 0.27$ mm/s. This doublet was interpreted by Vannice *et al.* (*9, 13*) as due to FeRu clusters located at the surface. The observation of surface and bulk material resonance lines arises from the extremely high asymmetric charge distribution of bimetallic clusters located at the surface. This effect was first observed by Garten (*2*) and arises only with highly dispersed bimetallic clusters. Thus, this effect cannot be observed, for example, with compact FeRu clusters because of the low-static surface component.

Lam and Garten (*53*) explain the high isomer shift of the doublet of ~0.25 mm/s for

zero-valent iron by a lowering of the electron density due to the higher effective atom volume of the surface atoms.

Messmer *et al.* (*54*) found evidence that surface atoms of extremely small metal particles (<2.5 nm) have positive charges of +0.05 due to screening effects, while the central atoms have a slightly negative charge. This effect, also, should become visible in a positive isomer shift which we indeed observed in this study for small particles.

Summarizing, we explain the quadrupole splitting of the surface component of the FeRu clusters which is represented by a doublet in the following way.

(1) A larger asymmetry of the charge distribution with the surface atoms due to their lower coordination number.

(2) A larger asymmetry of the charge distribution of the surface atoms being in direct contact with the support, caused by charge transfer from the support to the FeRu cluster. A charge transfer of this kind has been proposed recently by Morris *et al.* (*55*) for Ru/MgO. This explanation for the surface doublet would, again, support the existence of SMSI with the 5Fe5Ru/MHC catalysts.

(3) Paramagnetic spin relaxation of the surface phase. It is well known that the hexagonal bulk FeRu also has an EFG at room temperature corresponding to a quadrupole splitting of 0.21 mm/s and is, therefore, difficult to detect (singlet). Below the Néel temperature, which varies with the ruthenium content, the hexagonal FeRu, however, is antiferromagnetic showing a singlet at $H = 1.5$ T. The surface component should behave analogously, in accordance with the experiments.

The Debye temperature of Fe ($\geqq$13)% Ru is 502 K. This is striking because we are able to calculate the particle size of the clusters to be $d = 1.55$ nm by means of the surface statistics of van Hardeveld and Hartog (*56*) from the doublet component. Particles $\leqq$2 nm should have Debye temperatures around 250 K. By analogy with the FeO · MgO clusters the high Debye temperature points toward an extremely strong bond between the FeRu clusters and the support. In this case, however, this effect cannot be due, as in the case of Fe^{2+}, to the formation of clusters with MgO, but might be explained by a strong charge transfer from MgO to Ru. In addition, coupling effects may play a role because ruthenium has a Debye temperature of 600 K.

Finally, we wish to discuss the carbide and Fe^{3+} components of the low-temperature Mössbauer spectra. The unstable carbide, which was obtained as an intermediate species during the CO exposure of the 5Fe5Co/MHC samples, was identified as θ-$Fe_{3-x}Co_xC$ with $x \approx 0.07$. The extremely low Debye temperature of this θ-carbide points toward an extremely thin surface carbide "skin" on the Fe_3Co particles.

Quite different, however, are the situations with the 5Fe5Ni/MHC samples. The superparamagnetic carbide forming at 295 K could be identified on the basis of low-temperature Mössbauer spectra as highly disperse but rather stable χ-$Fe_{5-x}Ni_xC_2$ with $x \approx 0.37$. The hyperfine field at 4.4 K was 23.4 T instead of 25.2 T, which caused us, by analogy with the work of Unmuth *et al.* (*17*, *18*), to assume the incorporation of nickel. The high Debye temperature of 560 K can be explained here, again, as being due to the charge transfer, because the χ-carbide particles have a size of about 1.33 nm, determined by us from the sextet fraction (50%).

3. *Kinetics of H_2 Exposure as Determined from MES Measurements*

After determination of the Debye–Waller factors of some representative samples we were able to determine the kinetics of H_2 exposure, based on the relative fractions of the individual components in the Mössbauer spectrum extrapolated to 0 K. Some typical Mössbauer spectra are shown in Fig. 2.

The kinetics of the H_2 exposure of

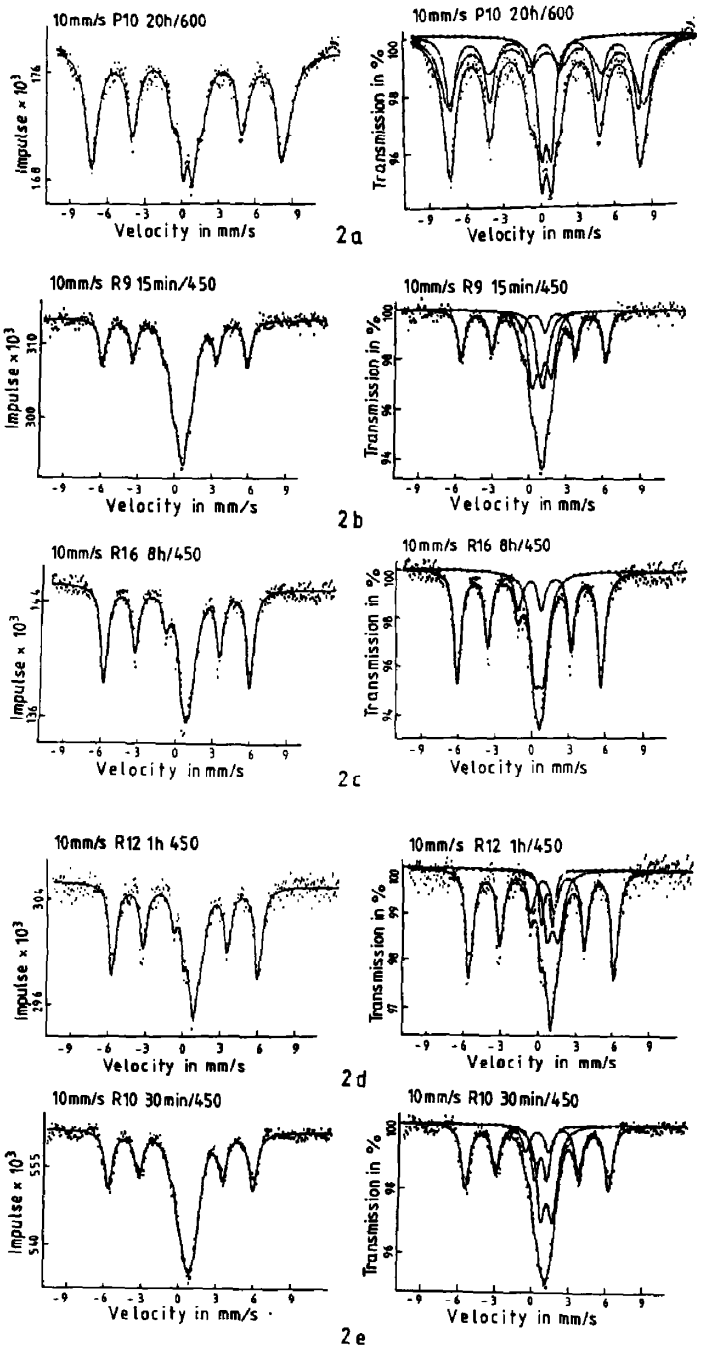

FIG. 2. MES of samples annealed for 20 h at 873 K and reduced at 723 K. Time of reduction, (a) 0 min, (b) 15 min, (c) 30 min, (d) 1 h, (e) 8 h.

the 5Fe5Co/MHC, 5Fe5Ni/MHC, and 5Fe5Ru/MHC samples are depicted in Figs. 3a–3i. Actually, we observe three different kinetics depending on the annealing temperature under argon at 673, 873, or 1073 K.

The kinetics of the H_2 exposure showed that the reduction of Fe^{3+} via Fe^{2+} as inter-

mediate product to the zero-valent iron is obtained with different alloys.

The time of reduction determined by the equilibrium between completely reduced iron and Fe^{2+} clusters varied considerably according to the alloying metal. The reduction time, however, was independent of the decomposition temperature under argon. For all 5Fe5Co/MHC samples the time of reduction was 7 h, for all 5Fe5Ni/MHC samples 4 h, and, finally, for all 5Fe5Ru/MHC samples 30 min. With the sample annealed at 873 K under argon an equilibrium between the different alloy phases was not established before 4 h.

Consequently, the particle size plays no important role for the velocity of reduction. In contrast, the alloying metal causes an acceleration of the reduction in a sequence which is expected on the basis of electrochemical potentials, i.e., Co < Ni < Ru. In the literature essentially longer reduction times are reported for supported iron, 20 to 24 h for Fe on MHC (*3*) and on TiO_2 (*26*), so

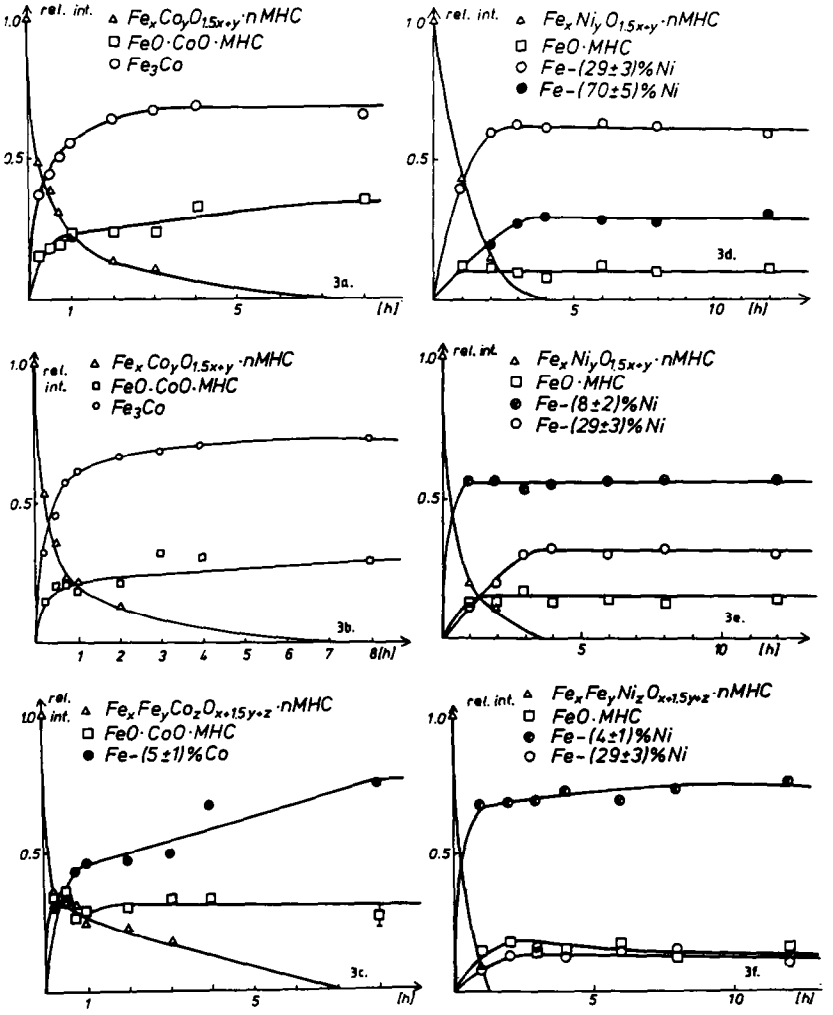

FIG. 3. Kinetics of reduction with H_2 at 723 K. (a) 5Fe5Co/MHC annealing at 673 K; (b) 5Fe5Co/MHC, 873 K; (c) 5Fe5Co/MHC, 1073 K; (d) 5Fe5Ni/MHC, 673 K; (e) 5Fe5Ni/MHC, 873 K; (f) 5Fe5Ni/MHC, 1073 K; (g) 5Fe5Ru/MHC, 673 K; (h) 5Fe5Ru/MHC, 873 K; (i) 5Fe5Ru/MHC, 1073 K.

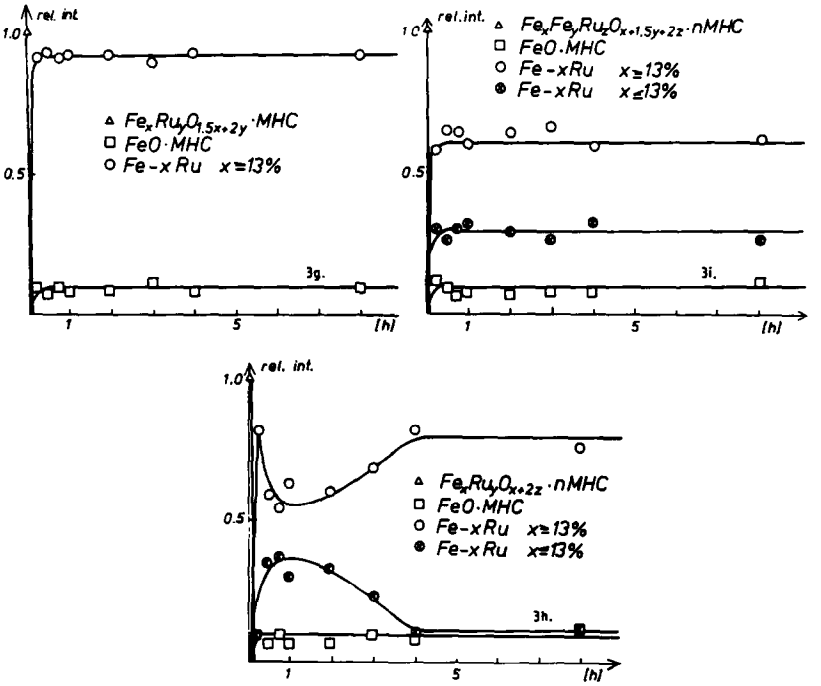

FIG. 3—*Continued.*

that the accelerating effect of the alloying metals can be characterized as being considerable.

The degree of reduction (ratio of Fe^0 to the total iron) also increases in the sequence Co < Ni < Ru. With 5Fe5Co/MHC it amounts to 67–75%, with 5Fe5Ni/MHC to 86–91%, and with 5Fe5Ru/MHC to about 94%. The residual iron which cannot be reduced further is present as Fe^{2+} in FeO · CoO or FeO · MHC clusters.

If one compares the samples with one and the same alloying metal with each other, it turns out that the degree of reduction increases with increasing annealing temperature, which, for its part, proceeds with increasing particle size.

The kinetics of the H_2 exposure of the 5Fe5Co/MHC catalysts, decomposed at 673 and 873 K (see Figs. 3a and 3b), differ only slightly in the degree of reduction (67 or 72%, respectively). With both samples the $Fe_xCo_yO_{1.5x+y}$ · *n* MHC is reduced to the Fe_3Co alloy or alloys close to this ordered alloy with a cobalt content of approximately 20 to 30%, corresponding to a hyperfine field splitting of 36.0 to 36.5 T.

Stanfield and Delgass (*19*), who investigated 4.87Fe5.13Co/SiO_2 samples, identified the alloy occurring after reduction as not quite ordered $Fe_{0.5}Co_{0.5}$. Besides this alloy no Fe^{2+} was present. Stanfield and Delgass could observe Fe^{2+} only with a higher iron : cobalt ratio. Consequently, for the stabilizing of Fe^{2+} in our samples the support which favors the Fe^{2+} cluster formation should be responsible. As, however, only alloys with a cobalt content of about 20 to 30% are obtained, although the iron : cobalt ratio of our samples was 1 : 1, it may be assumed that CoO forms clusters with an even higher tendency than FeO. The isomer shift of the FeO · CoO · MHC clusters is 0.76 and 0.84 mm/s, respectively (error ±0.5 mm/s). These values are distinctly lower than that of the Fe^{2+} clusters of the 5Fe5Ni/MHC samples which was δ = 1.12 mm/s. These isomer shifts correspond to the value of Fe^{2+} in the Fe/MgO samples which were investigated by

Boudart *et al.* (*3*). We suggest that the decrease in the isomer shift is due to electron transfer in the FeO · CoO · MHC clusters from Fe^{2+} to Co^{2+}. The absence of this effect with the 5Fe5Ni/MHC samples points to the fact that NiO plays a minor role in the formation of clusters. This conclusion seems to be plausible in view of the better reducibility of nickel than that of iron and cobalt.

The kinetics of the H_2 exposure of the 5Fe5Ni/MHC sample which had been decomposed previously at 673 K (see Fig. 3d) shows the formation of Fe–(29 ± 3)% Ni (Invar alloy) and Fe–(70 ± 5)% Ni. The Debye–Waller factors which we determined by means of low-temperature measurements are $f(295\ \text{K}) = 0.483$ and 0.876, respectively. Consequently, the kinetics determined at room temperature must be corrected considerably, so that we obtained 0.61 for the relative fraction of the Invar alloy and 0.29 for that of the Fe–(70 ± 5)% Ni alloy. The residual fraction of 0.10 was found to be Fe^{2+}, which could not be further reduced.

Reduction of the samples decomposed at higher temperatures (873 and 1073 K) (see Figs. 3e and 3f) mainly led to alloys with very low nickel contents nearly up to the phase separation found by Raupp and Delgass (*14*). The reduction curve (Fig. 3e) based on the sample decomposed at 873 K revealed a faster reduction of the ferrimagnetic $Fe_xNi_yO_{1.5x+y}$ particles to a bcc alloy of 8 ± 2% nickel content within at least 1 h: the superparamagnetic $Fe_xNi_yO_{1.5x+y}$ particles slowly reacted within 4 h to the Invar alloy which was preferred by these small particles. Therefore, the small particle size slowed down the reduction rate. The iron-rich alloy (Fe–(8 ± 2%) Ni) was represented by a sextet in MES with an average isomer shift of $\delta = 0.07 \pm 0.05$ mm/s, an average internal magnetic field of $\bar{H} = (33.8 \pm 0.2)$ T, and a relative content of nearly 56%. The single peak of the Invar alloy is related to a relative part of about 30%.

The results of the reduction of the sample decomposed at 1073 K (Fig. 3f) were similar to those discussed above.

The kinetics resulting from exposure of the 5Fe5Ru/MHC catalysts to H_2 (Figs. 3g–3i) show that with the sample annealed at 673 K under argon exclusively Fe–(≧13)% Ru alloy particles are formed beside the FeO · MgO clusters. With the samples pretreated at 873 and 1073 K, however, a phase separation into an Fe–(≧13)% Ru phase (sextet) takes place. This phase separation is partially reversible with the sample decomposed under argon. The iron-rich phase shows an average isomer shift of $\delta = 0.07 \pm 0.05$) mm/s and an average hyperfine field splitting of $H = (32.6 \pm 0.2)$ T. The decrease in the inner magnetic field by 0.4 T with respect to 33.0 T for α-Fe suggests a low (≦13)% ruthenium concentration. The ruthenium-rich alloy is represented in the Mössbauer spectrum by a singlet (bulk) and by a doublet (surface atoms) as we were able to demonstrate by means of low-temperature measurements (see above). From the ratio of volume to surface atoms we could determine the diameter d of the hexagonal Fe–(≧13)% Ru particles using the statistical calculations of van Hardenveld and Hartog (*56*).

From the kinetics of the H_2 exposure of the 5Fe5Ru/MHC samples (Figs. 3g–3i) and this particle size determination the following result:

1. H_2 exposure after annealing at 673 K under argon (see Fig. 3g). The $Fe_xRu_yO_{1.5+2y} \cdot n$MHC particles of 3.2 nm in size are reduced to FeO · MHC surface clusters between which completely reduced Fe–(≧13)% Ru clusters of about 2.5 nm segregate. These completely reduced bimetallic clusters are stable against sintering during the H_2 exposure at 723 K. We believe that the stability can be explained as follows. According to Wynblatt (*57*), for particles smaller than 4 nm the particle growth by migration dominates, in line with the diffusion and collision model of Pulvermacher and Ruckenstein (*58*). The diffusion

of the FeRu clusters on our samples, however, is hindered, on the one hand, by the surrounding FeO · MHC surface clusters and on the other by the drastic charge transfer from Mg to Ru at the interface between support and FeRu clusters. Thus, particles are quasi-fixed.

2. H_2 exposure after annealing at 1073 K under argon (Fig. 3i). From the $Fe_x^{II}Fe_y^{III}Ru_zO_{x+1.5y+2z}$ · MHC particles with an average diameter of 10 nm (from the sextet component) (see Table 1), Fe(≦13)% Ru clusters with $\bar{d} \approx 2.5$ nm are generated as well as essentially larger particles ($\bar{d} \gg 2.5$ nm), on which an iron-rich phase of Fe(≦13)% Ru has segregated on the surface.

Assuming that all particles show phase separation with a segregation of an iron-rich phase at the surface, the ruthenium-rich phase should not show any iron surface atoms. The corresponding Mössbauer spectrum should show no doublet due to these iron atoms, in contrast to the experimental findings. Therefore, we assume the coexistence of particles with and without phase separation. At the surface, indeed, the iron-rich alloy segregates due to the strong charge transfer from Mg^{2+} to Ru (*55*), under which an iron-rich layer remains. The small particles which show phase separation (as with the kinetics discussed previously) have a particle diameter of $d = 2.5$ nm, so we can adjust the critical particle diameter for the phase separation to be (2.5 ± 0.4) nm. Ponec (*59*) denoted 2.0–2.5 nm as the size range above which particle properties are determined by the bulk, and below which they are determined by the surface atoms. Above this critical size, phase separation occurs due to the metal–support interaction (MSI) and the different volatility of the metals.

3. H_2 exposure after annealing at 873 K under argon (Fig. 3h). Apparently, numerous particles have diameters only just above the critical value for phase separation. These particles with $d = \geqq 2.5$ nm segregate an iron-rich phase on their surface during the first 60 min of the H_2 exposure. Due to the higher volatility of the iron atoms (compared with that of ruthenium) which is further favored by the location on the surface (much smaller coordination number), the lower limit for the interparticle atom transport is exceeded, which should amount to 4 nm following Flynn and Wanke (*60*). From the iron-rich surface single iron atoms are dissolved out (the boiling point is drastically lowered for surface atoms); these iron atoms diffuse over the catalyst surface until they are absorbed again by another particle. The high volatility of the iron atoms is explained not only by the lowering of the boiling point of the surface atoms with lower coordination numbers, but also by the fact that for larger metal particles (≫2.5 nm) the surface atoms do not profit any longer by the "MSI" in the way that the smaller particles (<2.5 nm) will profit.

4. Kinetics of CO Exposure as Determined from MES Measurements

By analogy with the H_2 exposure we determined the kinetics resulting from CO exposure of the reduced samples after having extrapolated the relative concentration of the observed components in the Mössbauer spectrum to the conditions at 0 K.

The kinetics of the CO exposure of the 5Fe5Co/MHC, 5Fe5Ni/MHC, and 5Fe5Ru/MHC samples are depicted in Figs. 4a–4i.

The kinetics of the CO exposure of the 5Fe5Co/MHC samples (Figs. 4a–4c) show that we must distinguish among at least three reaction steps: first the dissociative adsorption of carbon monoxide and, second, during further reaction the dominating reduction of the metal surface which is partially oxidized by the dissociative adsorption. Simultaneously (third) the adsorbed carbon diffuses partially into the bulk of the metal particles (see Fig. 4c) forming carbides.

The θ-carbides formed from the Fe_3Co alloy and the absorbed carbon are unstable due to the high cobalt content and decom-

pose into Fe_3Co and surface carbon. On the contrary, the θ-carbides formed in the case of an iron-rich Fe–(5 ± 1)% Co alloy are stable. Stanfield and Delgass (*19*) showed that with cobalt concentrations above 25%, carbide formation is no longer possible. With lower cobalt concentration, on the contrary, they found ε'-carbides, without indicating the cobalt content and stability. The preferred generation of ε'-carbides with smaller iron particles on SiO_2 has already been documented by a series of authors (*15, 18, 19, 27*). This can be understood from the same hexagonal crystal structure of ε'-carbide and SiO_2. By the same reasoning however, cubic χ- and θ-carbides are stabilized on MgO (*15*).

The formation of surface oxide during the dissociative adsorption of CO is also described by other authors (*29, 31, 32, 61*).

During further CO exposure, the oxide phase on the surface increases, whereas the carbon diffuses into the inner volume in order to form bulk carbides. Niemants-

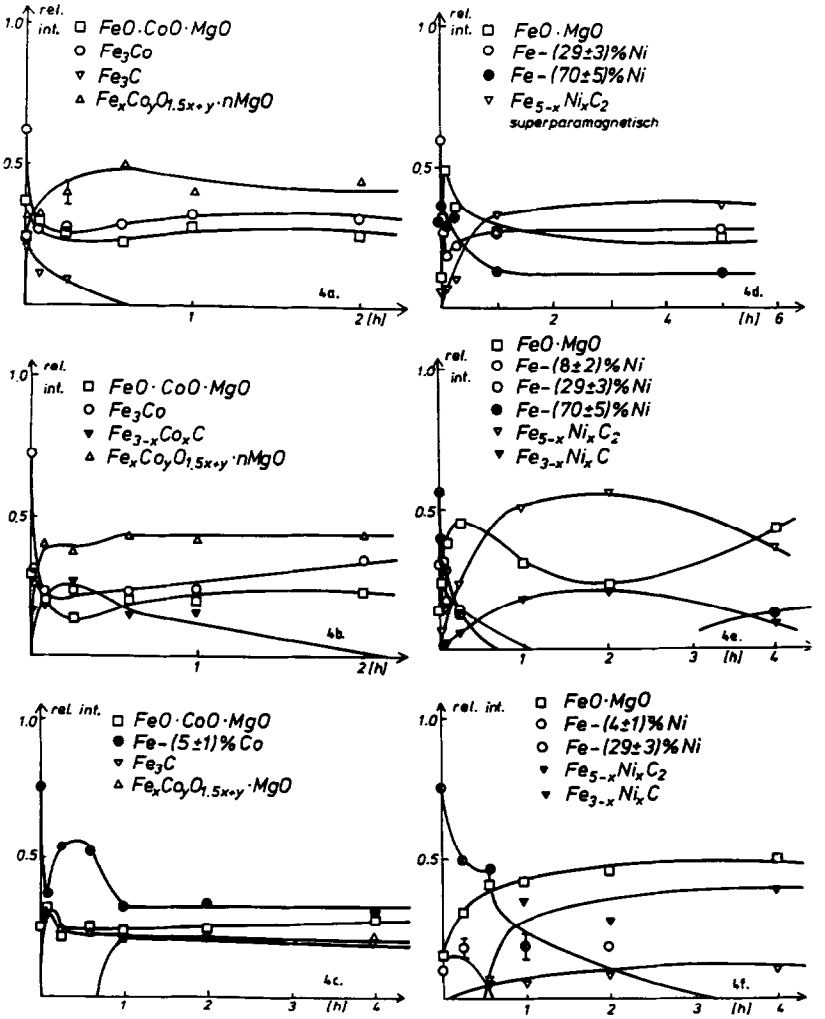

FIG. 4. Kinetics of carburization at 723 K. (a) 5Fe5Co/MHC annealing at 673 K; (b) 5Fe5Co/MHC, 873 K; (c) 5Fe5Co/MHC, 1073 K; (d) 5Fe5Ni/MHC, 673 K; (e) 5Fe5Ni/MHC, 873 K; (f) 5Fe5Ni/MHC, 1073 K; (g) 5Fe5Ru/MHC, 673 K; (h) 5Fe5Ru/MHC, 873 K; (i) 5Fe5Ru/MHC, 1073 K.

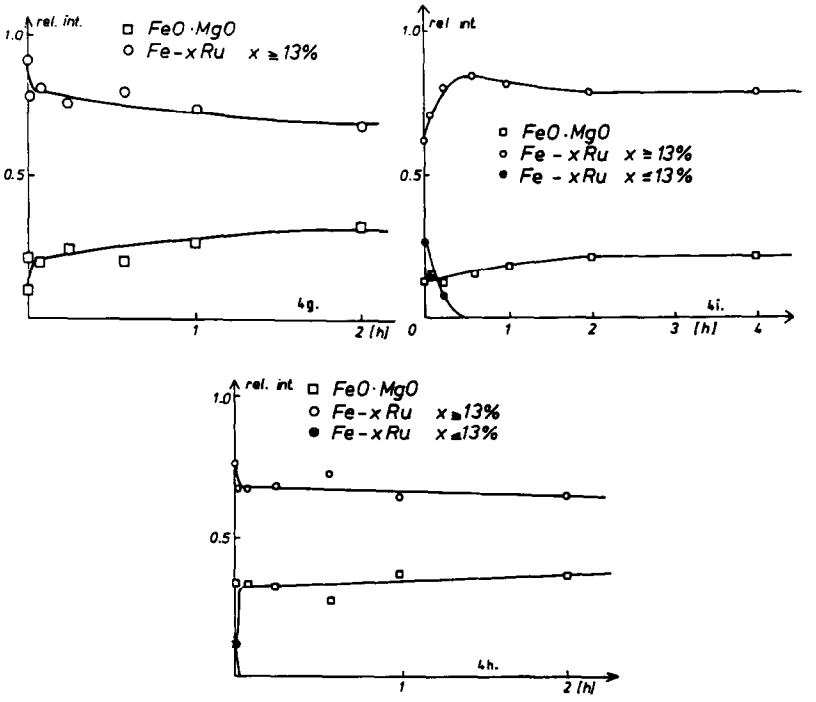

FIG. 4—*Continued.*

verdriet *et al.* (*29, 31*) concluded from the ratio of oxide to carbide, which was 11 : 4 for the unsupported iron exposed to CO, that the formation of surface oxide layers inhibits the carbon diffusion so that the carbide formation proceeds only slowly. In this case inactive surface carbon is generated.

The following picture results. The kinetics of the CO exposure of the 5Fe5Co/MHC sample annealed at 673 K under argon and reduced at 723 K under H_2 (see Fig. 4a) shows that within 1 min the dissociative adsorption of the carbon has altered the total metal surface. $Fe_x^{III}Co_y^{II}O_{1.5x+y}$ (0.32 rel[e]) as well as θ-Fe_3C (0.20 rel[e]) are generated on the metal surface. The relative fraction of the Fe_3C alloy decreases from 0.63 to 0.24. As the ratio of Fe^{2+} in the FeO · CoO · MgO clusters also decreases, the iron(III) oxide seems to form not only on the metal surface but also within the quasi-two-dimensional Fe^{2+} surface clusters. The isomer shift of the residual Fe^{2+} ions increases from $\bar{\delta}$ = (0.77 ± 0.05) to (1.00 ± 0.05) mm/s. We wish to explain the low isomer shift of δ = 0.77 mm/s for Fe^{2+} by an electron transfer from Fe^{2+} to Co^{2+} within the clusters.

This effect is compensated by the CO adsorption as now the electrons take part in the Fe–C bond.

Between 5 and 30 min after the beginning of the CO exposure (see Fig. 4d) the unstable surface carbide decomposes and the iron oxidizes. Consequently, the iron(III) oxide ratio increases to a relative fraction of 0.50 after 35 min of CO exposure. Thereafter, parts of the metal surface regenerate according to $O_{(s)} + CO_{(s)} \rightarrow CO_{2(g)}$. Thus, the iron(III) oxide ratio decreases to 0.42.

The rather low Debye temperature (θ_D = 179 K) and the complete superparamagnetism (at 295 K) of the $Fe_x^{III}Co_yO_{1.5x+y}$ on the other hand suggest particle sizes of about 2 nm (surface statistics!).

The kinetics of the CO exposure of the 5Fe5Co/MHC sample decomposed at 873

K (see Fig. 4b) shows due to the slightly larger particles a deviating behavior concerning the carbide formation. After 1 min, again, θ-Fe_3C has formed on the surface of the metal particles exhibiting the same Mössbauer parameters (δ = 0.20 mm/s, H = 20.86 T, and rel^e = 0.16) within the limits of experimental error as the 5Fe5Co/MHC sample, pretreated at 673 K and exposed to CO for 1 min. However, the hyperfine field H decreases during further reaction from 20.86 to 20.08 T, which may be a hint for the formation of cobalt-containing θ-$Fe_{3-x}Co_xC$ structures, caused by the carbon diffusion into the inner volume. Because of their cobalt content, however, these structures are unstable and decompose after 120 min of CO exposure.

The kinetics of the CO exposure of the 5Fe5Co/MHC sample (treated for 20 h/1073 K/Ar and 8 h/723 K/H_2), containing the iron-rich Fe–(5 ± 1)% Co alloy (see Fig. 4c), shows a minor degree of oxidation (0.21 rel^e). Two factors are responsible: first the regenerative reduction of the surface oxide starts already after 5 min instead of 35 min CO exposure, and second the θ-Fe_3C that forms between 45 and 60 min is stable. The hyperfine fields of this θ-Fe_3C with 20.83 to 20.99 T exclude an incorporation of cobalt, which explains the stability of the carbides.

A comparison of the kinetics of the CO exposure of the 5Fe5Co/MHC catalysts with that of the 5Fe5Ni/MHC samples (see Figs. 4d–4f), which were measured under the same conditions, reveals some interesting differences:

1. The oxidation of the metal surface of the Ni-rich alloys shows no formation of Fe^{3+}, but causes only the FeO ratio to increase. We assume the adsorbed oxygen to be removed by CO, before an Fe–O bond can be formed. In the case of an Fe–O bond formation, it should be relatively weak due to the electron transfer from Fe to neighboring Ni atoms, so that the reduction with further CO should proceed more easily.

2. With the 5Fe5Co/MHC samples bulk carbides form with Debye temperatures of θ_D = 560 K which are typical for the bulk material. Only the kinetics (see Fig. 4f) reveal a retardation of carbide formation of 35 min, correlated with the drastic surface oxide formation with this sample.

3. The smaller particle size of the iron–nickel alloys of the 5Fe5Ni/MHC samples annealed at 673 and 873 K (see Figs. 4d and 4e) favors the formation of the more carbon-rich χ-carbide ($Fe_{5-x}Ni_xC_2$). Numerous authors (*15, 18, 19, 27*) report that smaller particles form more carbon-rich carbides. The reason for that cannot be attributed to the carbon diffusion as the diffusion coefficient for carbon in α-iron is, for example, 10^{-4} mm^2/s. The reason is that small particles have many edge and corner atoms which are able to adsorb two CO molecules at the same time.

4. The generated iron–nickel mixed carbides are rather stable. Only the kinetics of the CO exposure of the sample pretreated at 873 K (see Fig. 4e) shows carbide decomposition between 2 and 4 h. The formation of iron–nickel mixed carbides was already detected by Unmuth *et al.* (*18*) with 4Fe : Ni/SiO_2 catalysts. We can confirm the statement of Unmuth *et al.* that the decrease in the hyperfine field in mixed carbides of that kind is a function of the alloy metal concentration. Table 3 shows the

TABLE 3

CO Exposure Time up to the Maximum Carbide Ratio (%)

Temperature of heating (K)	Catalyst	
	5Fe5Co/MHC	5Fe5Ni/MHC
673	1 min 20%	1 h 33%
873	15 min 27%	2 h 77%
1073	60 min 22%	4 h 50%

time necessary to obtain the maximum carbide ratio to be dependent on the particle size (decomposition temperature) and the stability of the carbides.

Considering now the time-dependent behavior of the 5Fe5Ru/MHC samples pretreated at 673 and 873 K, one can recognize that the iron(II) surface oxide formation is nearly terminated within the first 5 min of CO exposure: the FeO ratio increases from 0.09 to 0.21 (see Fig. 4g) and from 0.12 to 0.33 rel., respectively, in Fig. 4h. Determining the particle size according to the surface atom data for hcp structures (*56*) from the ratio of doublet (surface atoms) to singlet (bulk material) intensities of the MES of the Fe–(≦13)% Ru alloy, we must assume a decrease in the particle size in the FeRu clusters from about 2 to 1 nm. This suggests a redispersion, as proposed by the mechanism of Wang and Schmidt (*52*). The iron(II) surface oxide induces a redispersion within the particles due to the formation of a void at the metal/metal oxide boundary and on account of the different interactions of metal oxide and support, on the one hand, and metal and support on the other. As a consequence of these processes "cross section" occurs, i.e., iron(II) oxide precipitates in the neighborhood of metal particles thus forming two-dimensional FeO · MgO clusters with the support.

A different picture is shown by the kinetics of the CO exposure of the 5Fe5Ru/MHC sample (see Fig. 4i), annealed at 1073 K. Here a remixture of the two iron alloy phases takes place by redispersion. The redispersion effect is much stronger than that with the other two samples (from 2.49 to 0.66 nm after 4 h).

The iron(II) oxide component is changing during the first 35 min only within the limits of experimental error of ±0.02 (see Fig. 4i); the particle size, d_a, however, during that period decreases from 2.49 to 1.23 nm (i.e., the volume decreases to $\frac{1}{8}$), so another redispersion mechanism should be assumed.

Wang and Schmidt (*52*) already assumed that other compounds like carbide, etc., can also substitute for the oxide in this model.

We explain the data (Fig. 4i) as follows. Ruthenium can more easily chemisorb CO than iron and diffuses rapidly at the surface. This results in an intermixing of the iron-rich and the ruthenium-rich phases. On the surface a carbon-rich layer forms (adsorbed and possibly also incorporated carbon) and according to Wang and Schmidt's model "cross section" occurs, as the Ru–C bond strength can be increased by the charge transfer from Mg^{2+} to Ru.

The chemisorption is explained by the Blyholder model (*61*) as a donor–acceptor mechanism, according to which the binding is achieved by electron transfer from the highest occupied orbital of CO to the metal and by "back-donation" of the electrons of the metal to the lowest unoccupied orbital of the CO. This "back-donation" can be strengthened by the ruthenium, diminishing the electron density of the iron (*5*) or the Mg^{2+} (*55*) by transferring electron density into the π^*-orbital of the CO. Another determining force for the redispersion is that first a decrease in the particle size below 100 atoms (a cluster diameter of 1.23 nm corresponds to a cluster of 82 atoms in the case of the hcp structure) leads to a larger charge density per ruthenium atom and second increases the number of ruthenium atoms located at edges and corners to which the C atom can approach (shorter Ru–C bond length). These effects, again, stimulate the "back-donation."

CONCLUSION

From our results, a schematic model of the 5Fe5Me catalysts on magnesium hydroxide carbonate (MHC) can be developed (Fig. 5). Summarizing, we explain our model briefly as follows.

(a) After the ion exchange reaction one obtains Fe and Me salts ($Fe(NO_3)_3 \cdot 9H_2O$, for example), standing in loose contact with the support. The particle size of the metal salt is independent of the kind of metal salt

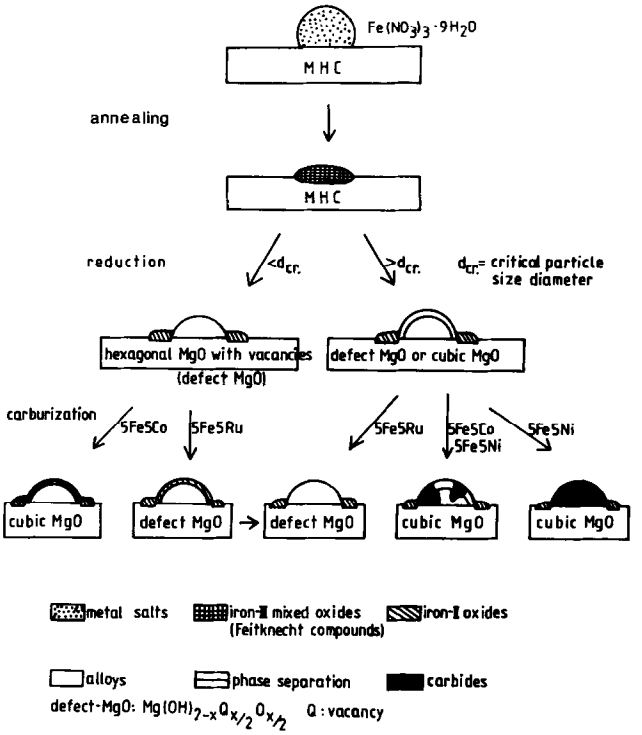

FIG. 5. Schematic diagram of the formation of 5Fe5Me catalysts supported on magnesium hydroxide carbonate (MHC).

and the same precipitation conditions lead to one and the same completely reproducible particle size (same BET surface area).

(b) Annealing under argon results in a diversification of the particle size as a function of the temperature and the strength of the MSI (metal support interactions). The MSI can be explained in this case as a diffusion of magnesium hydroxide carbonate into the basic metal oxides which form during the annealing under argon. As a result of this process the so-called Feitknecht compounds form: $Mg^{II}_{w}Fe^{i}_{x}Me^{j}_{y}(OH^{-})_{2w+ix+jy-2z}(CO_3^{2-}) \cdot nH_2O$. From the Mössbauer spectra we could detect an increase in the MSI in the sequence Fe $\leqq$ Co < Ni $\ll$ Ru. (Increasing inhomogeneities led to a decrease in the hyperfine field.) The Feitknecht compounds are supposed to be embedded into the support.

(c) The H_2 exposure causes the intraparticle decomposition of the Feitknecht compounds into quasi-two-dimensional Me^{2+} support surface clusters and completely reduced metal particles, which possibly prefer a hemispherical form because of the minor surface energy. The FeMe clusters are stable against annealing as the surrounding Me^{2+} support surface clusters and electronic MSI (charge transfer) inhibit a migration. Above a critical particle diameter, with regard to phase separation, a segregation of a metal phase enriched with an alloy metal takes place. The reason for the phase separation is the different MSI of the metals in the alloy. These MSI effects are of an electronic nature (charge transfer). The critical particle diameter d_{cr} is a function of the difference of the MSI strength of the alloy metals: d_{cr}(Fe/Co) $\approx$ (10 $\pm$ 2) nm, d_{cr}(Fe/Ni) < 6.5 nm, d_{cr}(Fe/Ru) = (2.5 $\pm$ 0.4) nm. The MSI of the metals grow, therefore, in the sequence Fe $\leqq$ Co < Ni < Ru.

(d) In a CO atmosphere the small alloy clusters are oxidized at the surface. The degree of oxidizability depends on the metals

of the alloy. On the surface of FeCo clusters the iron oxidizes up to Fe^{3+}, whereas on the surface of FeNi and FeRu clusters the iron oxidizes only up to Fe^{2+}. The formation of surface metal oxides on the FeMe clusters leads to an intraparticle redispersion according to the model suggested by Wang and Schmidt (*52*). By that, first the smaller Fe–Me clusters without phase separation become still smaller and, second, by the "cross section" effect they are freed from the surface oxide. The oxides precipitate next to the Fe–Me clusters, enlarging the number of the two-dimensional Me^{2+} support clusters already existing. The surface of the Fe–Me clusters is inactivated during the CO exposure by immobile carbon (graphite layer) or mobile carbon (triple carbon-to-ruthenium bond) for further oxidation.

Besides the surface oxide unstable surface carbide also forms with the FeCo/MHC catalysts.

The larger particles with a tendency to phase separation form "bulk" carbides by carbon diffusion into the metal particles. These "bulk" carbides form phases within the metal particles or extend over the whole metal particle. The carbided particles show no redispersion, thus emphasizing the difference in size from the particles mentioned before which exhibit a redispersion.

An exception are the FeRu/MHC catalysts exhibiting phase separation. The iron-rich Fe–($\leqq$13)% Ru phase, also, is not able to form carbides. As the Ru–C bonding is energetically particularly favorable, Ru atoms diffuse to the surface thus compensating the phase separation.

The strengthening of the Ru–C bonding by MSI leads to the redispersion, for example, of $\frac{1}{8}$ of the volume, similar to that of the surface oxide. If surface oxide occurs additionally, the volume can decrease from its original 682 atoms to 12 atoms, as we observed with one sample.

REFERENCES

1. Garten, R. L., and Ollis, D. F., *J. Catal.* **35,** 232 (1974).
2. Garten, R. L., *J. Catal.* **43,** 18 (1976).
3. Boudart, M., Delbouille, A., Dumesic, J. A., Khammouma, S., and Topsøe, H., *J. Catal.* **37,** 486 (1975).
4. Vannice, M. A., Lam, Y. L., and Garten, R. L., *Amer. Chem. Soc. Div. Pet. Chem. Prepr.* **23,** 495 (1978).
5. Ott, G. L., Fleisch, T., and Delgass, W. N., *J. Catal.* **60,** 394 (1979).
6. Ott, G. L., Fleisch, T., and Delgass, W. N., *J. Catal.* **65,** 253 (1980).
7. Reed, P. D., Comrie, C. M., and Lambert, R. M., *Surf. Sci.* **59,** 33 (1976).
8. Wise, H., and McCarty, J. G., *Surf. Sci.* **133,** 311 (1983).
9. Vannice, M. A., Lam, Y. L., and Garten, R. L., *in* "Advances in Chemistry Series," Vol. 178, p. 25. Amer. Chem. Soc., Washington, DC, 1979.
10. Niemantsverdriet, J. W., van Kaam, J. A. C., van der Kraan, A. M., and van Loef, J. J., *in* "Proceedings of the International Conference on the Applications of the Mössbauer-Effect, Alma Ata, 1983.
11. Guczi, L., *Catal. Rev. Sci. Eng.* **23,** 329 (1981).
12. Dezsi, I., Nagy, D. L., Eszterle, M., and Guczi, L., *J. Phys. Colloq. C* **2,** 40, 76 (1979).
13. Vannice, M. A., and Garten, R. L., *in* "Scientific Problems of Coal Utilization. Proceedings of a Conference, Morgantown, WV, 1977." Technical Information Center, Washington, DC.
14. Raupp, G. B., and Delgass, W. N., *J. Catal.* **58,** 337 (1979).
15. Raupp, G. B., and Delgass, W. N., *J. Catal.* **58,** 348 (1979).
16. Raupp, G. B., and Delgass, W. N., *J. Catal.* **58,** 361 (1979).
17. Unmuth, E. E., Schwartz, L. H., and Butt, J. B., *J. Catal.* **61,** 242 (1980).
18. Unmuth, E. E., Schwartz, L. H., and Butt, J. B., *J. Catal.* **63,** 404 (1980).
19. Stanfield, R. M., and Delgass, W. N., *J. Catal.* **72,** 37 (1981).
20. Arcuri, K. B., Schwartz, L. H., Piotrowski, R. D., and Butt, J. B., *J. Catal.* **85,** 349 (1984).
21. Jiang, X. Z., Stevenson, S. A., Dumesic, J. A., Kelly, T. F., and Casper, R. J., *J. Phys. Chem.* **88,** 6191 (1984).
22. Yoshioka, T., Koezuka, J., and Ikoma, H., *J. Catal.* **16,** 264 (1970).
23. Bianchi, D., Borcar, S., Teulé-Gay, F., and Bennett, C. O., *J. Catal.* **82,** 442 (1983).
24. Bianchi, D., Tau, L. M., Borcar, S., and Bennett, C. O., *J. Catal.* **84,** 358 (1983).
25. Tau, L. M., Borcar, S., Bianchi, D., and Bennett, C. O., *J. Catal.* **87,** 36 (1984).
26. Tau, L. M., and Bennett, C. O., *J. Catal.* **89,** 285 (1984).
27. Amelse, J. A., Butt, J. B., and Schwartz, L. H., *J. Phys. Chem.* **82,** 558 (1978).

28. Niemantsverdriet, J. W., and van der Kraan, A. M., *J. Catal.* **72,** 385 (1981).
29. Niemantsverdriet, J. W., van der Kraan, A. M., van Dijk, W. L., and van der Baan, H. S., *J. Phys. Chem.* **84,** 3363 (1980).
30. Vannice, M. A., *J. Catal.* **37,** 462 (1975).
31. Niemantsverdriet, J. W., Elipse, C. F. J., van der Kraan, A. M., and van Loef, J. J., *Appl. Surf. Sci.* **10,** 302 (1982).
32. van der Kraan, A. M., and Niemantsverdriet, J. W., *in* "Proceedings of the International Conference on the Applications of the Mössbauer-Effect, Alma Ata, 1983.
33. Somorjai, G. A., "Chemistry in Two Dimensions: Surfaces," p. 170. Cornell Univ. Press, Ithaca, NY, 1981.
34. Niemantsverdriet, J. W., Flipse, C. F. J., Selman, B., van Loef, J. J., and van der Kraan, A. M., *Phys. Lett. A* **100,** 445 (1984).
35. Niemantsverdriet, J. W., van der Kraan, A. M., and Delgass, W. N., *J. Catal.* **89,** 138 (1984).
36. Berry, F. J., and Maddock, A. G., *Inorg. Chim. Acta* **37,** 255 (1979).
37. Petrera, M., Gubitosa, G., Gennaro, A., Burriesci, N., and Airoldi, F., *Gazz. Chim. Ital.* **110,** 465 (1980).
38. Kock, A. J. H. M., Fortuin, H. M., and Geus, J. W., *J. Catal.* **96,** 261 (1985).
39. Martens, R., Gentsch, H., and Freund, F., *J. Catal.* **44,** 366 (1976).
40. Freund, F., *Ber. Deut. Keram. Ges.* **52,** 53 (1975).
41. Mørup, S., and Thrane, N., *Chem. Phys. Lett.* **21,** 363 (1973).
42. Krupianskii, Yu. F., and Suzdalev, I. P., *Sov. Phys. JETP* **38,** 859 (1974).
43. Kündig, W., Bömmel, H., Constabaris, G., and Lindquist, R. H., *Phys. Rev.* **142,** 327 (1966).
44. Hobson, M. C., and Gager, H. M., *J. Catal.* **16,** 254 (1970).
45. Simkin, D. J., Ficalora, P. J., and Bernheim, R. A., *Phys. Lett.* **19,** 536 (1965).
46. Bhide, V. G., and Tambe, B. R., *J. Mater. Sci.* **4,** 955 (1969).
47. Shirane, G., Cox, D. E., and Ruby, S. L., *Phys. Rev.* **125,** 1158 (1962).
48. Jung, H. J., Vannice, M. A., Mulay, L. N., Stanfield, R. M., and Delgass, W. N., *J. Catal.* **76,** 208 (1982).
49. Niemantsverdriet, J. W., van der Kraan, A. M., Delgass, W. N., and Vannice, M. A., *J. Phys. Chem.* **89,** 67 (1985).
50. Travis, J. C., *in* "An Introduction to Mössbauer Spectroscopy" (L. May, Ed.). Plenum, New York, 1971.
51. Benziger, J. B., and Larson, L. R., *J. Catal.* **77,** 550 (1982).
52. Wang, T., and Schmidt, L. D., *J. Catal.* **70,** 187 (1981).
53. Lam, Y. L., and Garten, R. L., *in* "Proceedings, the 6th Ibero-American Symposium on Catalysis, Rio de Janeiro, 1978.
54. Messmer, R. P., Knudson, S. K., Johnson, K. H., Diamond, J. B., and Yang, C. Y., *Phys. Rev.* **813,** 1396 (1976).
55. Morris, S. R., Moyes, R. B., Wells, P. B., and Whyman, R., *J. Catal.* **96,** 23 (1985).
56. van Hardeveld, R., and Hartog, F., *Surf. Sci.* **15,** 189 (1969).
57. Wynblatt, P., *in* "Growth and Properties of Metal Clusters" (J. Bourdon, Ed.). Elsevier, Amsterdam, 1980.
58. Pulvermacher, B., and Ruckenstein, E., *J. Catal.* **35,** 115 (1974).
59. Ponec, V., *in* "Metal–Support and Metal–Additive Effects in Catalysts" (Symposium, Ecully, 1982) (B. Imelik *et al.*, Eds.), p. 1. Elsevier, Amsterdam, 1982.
60. Flynn, P. C., and Wanke, S. E., *J. Catal.* **34,** 390 (1974).
61. Blyholder, G. J., *J. Phys. Chem.* **68,** 2772 (1964).